Chapter - 5

Effect of L-Leucine on Structural, Thermal, Electrical and Optical Properties of Potassium Dihydrogen Phosphate (KDP)

Chapter-5: Effect of L-Leucine on Structural, Electrical and Optical Properties of Potassium Dihydrogen Phosphate (KDP) Crystals

1. Introduction:

Nowadays, there is a huge demand for electro-optical devices, data storage devices, optical signal processing, etc., in a vast range of technological applications. The non-linear optical [NLO] materials are an important class of materials that fulfil this demand due to their properties like high damage threshold, frequency doubling, wide transparency range, phase, and amplitude modulations, etc. Applications in optoelectronics, telecommunications, laser technology and optical storage devices require materials with high optical non-linearity. The water-soluble crystals containing complex organic molecules have attracted extensive interest in the last few years [1]. Potassium Dihydrogen Phosphate (KDP) and Ammonium Dihydrogen Phosphate (ADP) are well-known and important materials with non-linear properties. These materials are favoured for good electro-optical applications and are especially useful for various non-linear optical applications using intense lasers like Nd: YAG. Due to the KDP crystal's piezo-electric (anti-ferroelectric at low temperature) and non-linear properties, the crystal finds a wide range of integrated and non-linear optical applications [2,3].

For some years, KDP has been the topic of a wide range of investigations due to its intriguing electrical and optical properties, structural phase transitions and ease of crystallization. As amino acids possess a proton donor carboxy acid (-COOH) group and a proton acceptor amino ($-NH_2$) group, they assume intriguing roles in materials for NLO applications [4]. The inclusion of amino acids in KDP greatly influences the optical properties and SHG (Second Harmonic Generation) efficiency [5, 6]. KDP belongs to the scalenohedral (twelve faced) class of the tetragonal crystal system [7]. Some organic crystals possess special properties, particularly large optical non-linearity, and low cut-off wavelength in the UV region; therefore, the organic NLO crystals are also useful in optical devices. However, organic crystals have limitations, such as poor mechanical and thermal stability. To overcome these problems, the combination of organic and inorganic hybrid compounds can lead to a new class of materials called "semi-organic" materials having large optical non-linearity, higher mechanical strength and chemical stability [8]. The influence of additives such as amino acids on KDP crystal formation and habit modification has been investigated [9,10]. According to some reports, the inclusion of certain amino acids as dopants improves the non-linear and piezo-electric

characteristics of materials [11]. KDP crystals doped with amino acids have been reported to be potential NLO active materials [12-17]. However, the development and characteristics of single crystals of L-Leucine doped KDP have not been found in the reported literature. L-Leucine is a branched-chain amino acid at neutral pH with a non-linear aliphatic sidechain that takes on a zwitterionic state [18]. L-Leucine (1 mol% and 2 mol%) doped KDP crystals were produced at room temperature using a slow evaporation method and subjected to Powder X-ray Diffraction (XRD), Dielectric Analysis, Fourier Infrared Transform Spectroscopy (FTIR), Photoluminescence (PL) Analysis, UV-Visible (UV-Vis) Spectroscopy and Relative SHG Efficiency test.

2. Experimental details:

The slow evaporation technique was used to grow pure and L-Leucine (1 mol% and 2 mol%) doped KDP crystals. A detailed discussion of the evaporation method of the solution growth process has been given in chapter-3.

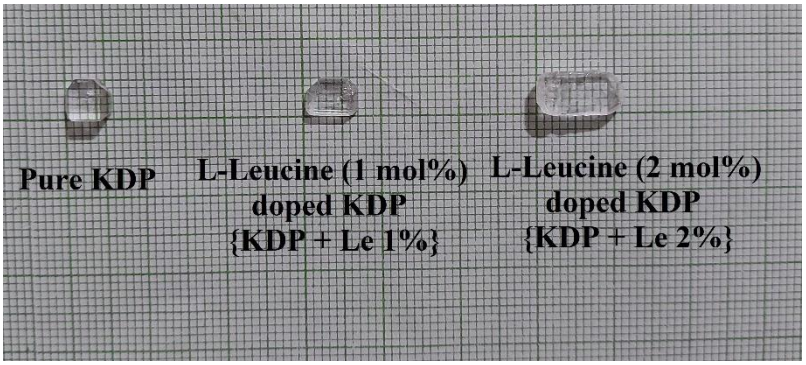

Figure 1. Grown crystals of pure KDP and L-Leucine doped KDP

3. Results and Discussion:

3.1 Powder X-ray Diffraction (XRD) Analysis:

Powder X-ray diffraction analysis was used to examine the crystalline state of fine powdered L-Leucine doped KDP crystals as well as of pure KDP crystals. As shown in figure 2(a), the sharp peaks obtained from XRD plots indicate the good crystallinity of the material. The most prominent peaks observed in the XRD plots are (100), (200), (112), (121), (220), (301) and (132). The XRD patterns of L-Leucine doped KDP crystals are identical to those obtained for pure KDP, indicating that no new phase occurs, and the crystals retain the tetragonal system, indicating that the dopant incorporation does not affect the doped KDP crystal structure. Table 1 shows the calculated values of lattice parameters of L-Leucine (1 mol% and 2 mol%) doped

KDP crystals and pure KDP. These parameters were found with the help of FullProf Suite software and are well-matched with the result obtained for pure KDP with symmetry space group $I\bar{4}2d$, indicating that L-Leucine enters the KDP lattice. However, it is observed that doping concentration does not significantly change the lattice parameters. It is found that the intensity of diffracted peaks varies. The different sizes and orientations of the powered grains can be attributed to the variations in peak amplitude. The addition of dopants causes the shifting of certain prominent peaks, as shown in figure 2 (b). However, in terms of the instrument resolution, this shift can be considered insignificant. The lattice generated by amino acid accommodation in the KDP lattice might be the source of this change. The change in structural characteristics of pure KDP and L-Leucine (1 mol% and 2 mol%) doped KDP crystals is shown in table 2.

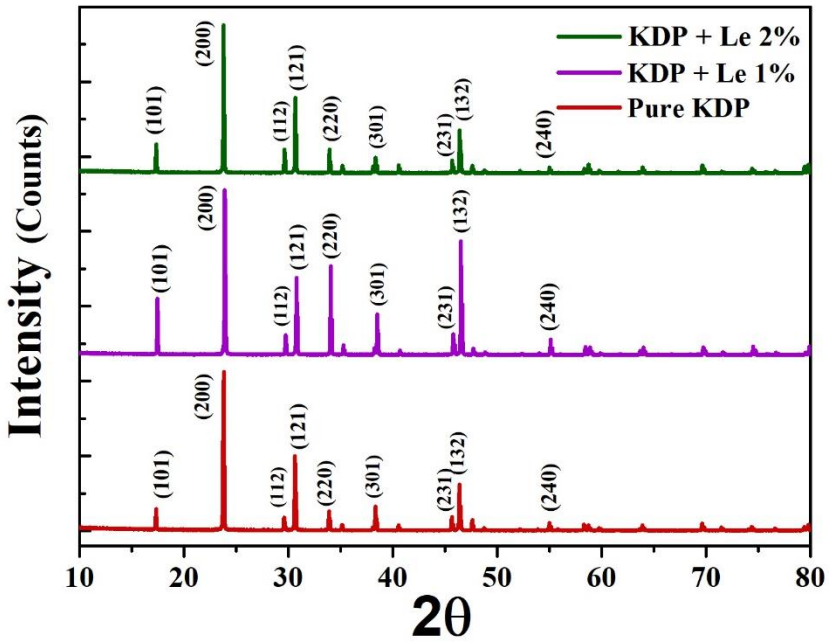

Figure 2(a). Powder XRD plots of Pure and L-Leucine doped KDP crystals.

Table 1. Lattice parameters of pure & L-Leucine doped KDP crystals

Crystals	a (Å)	b (Å)	c (Å)	Volume	Symmetry
Pure KDP (Reported)	7.448	7.448	6.977	387.033	Tetragonal
KDP + Le 1%	7.459	7.459	6.982	388.455	
KDP + Le 2%	7.453	7.453	6.979	387.663	

Table 2. Structural parameters of pure and L-Leucine doped KDP crystals

Sample	FWHM	2θ	Crystallite Size t (nm)	Strain ε ($lin^{-2}\,m^{-4}$)	Dislocation Density δ ($lin\,m^{-4}$)
Pure KDP	0.09	17.34	1.57	2.20E-02	2.82E-02
	0.11829	23.81	1.18	2.92E-02	4.97E-02
KDP + Le 1%	0.1025	17.35	1.38	2.51E-02	3.65E-02
	0.09648	23.94	1.45	2.38E-02	3.30E-02
KDP + Le 2%	0.08137	17.48	1.74	1.99E-02	2.30E-02
	0.0955	23.82	1.48	2.34E-02	3.17E-02

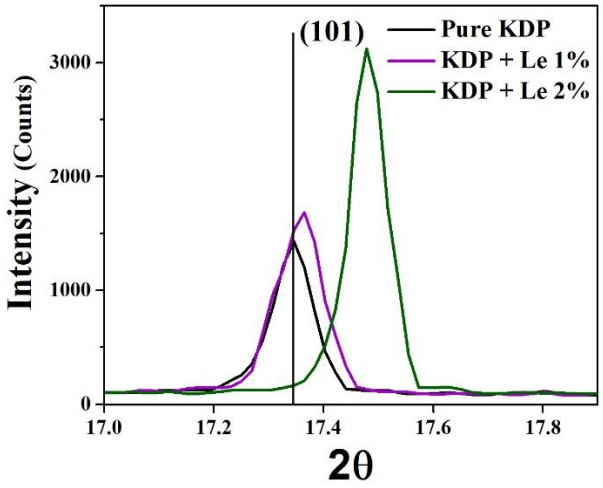

Figure 2(b). Peak (101) shifting of pure, and L-Leucine doped KDP crystals

3.2 Dielectric Analysis:

Each dielectric material has its own set of electrical properties determined by its dielectric or insulation characteristics. At different temperatures, the dielectric constant and dielectric loss of pure KDP and L-Leucine (1 mol% and 2 mol%) doped KDP crystals were measured in the frequency range of 100 Hz to 1 MHz. Figures 3(a-b) and 4(a-b) illustrate the frequency dependence of the dielectric constant and dielectric loss of pure and L-Leucine (1 mol% and 2 mol%) doped KDP crystals at various temperatures. The results show that when frequency increases, both the dielectric constant and dielectric loss decrease; however, both the dielectric parameters seem to increase with temperature. The presence of space charge polarisation at the grain boundary interfaces causes a high dielectric constant and dielectric loss at low frequencies depending on the purity and perfection of the sample [19]. The dielectric

properties of crystals are linked to their electro-optic properties, especially when they are nonconducting materials [20]. At high frequency, the low dielectric constant value reveals that crystal has high optical quality with fewer defects which is a desirable property of NLO applications [21, 22]. The dielectric constant's frequency dependence at different temperatures indicates that the dielectric constant values are almost temperature invariant at high frequencies but become more temperature sensitive as the frequency decreases. The dielectric constant is high at 373 K and low at 323 K at low frequencies. The dipoles may easily switch alignment with the changing field at low frequencies. The dipoles become less able to spin and hold phase with the applied field as the frequency increases, reducing their contribution to polarisation.

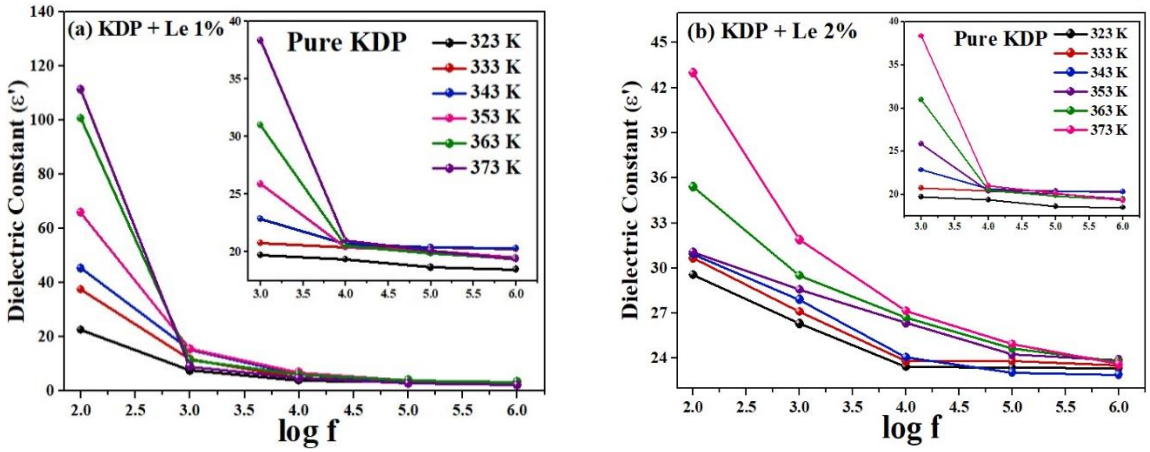

Figures 3. (a) Variation of dielectric constant with the frequency of L-Leucine (1 mol%) doped KDP crystal and **(b)** Variation of dielectric constant with the frequency of L-Leucine (2 mol%) doped KDP crystal.

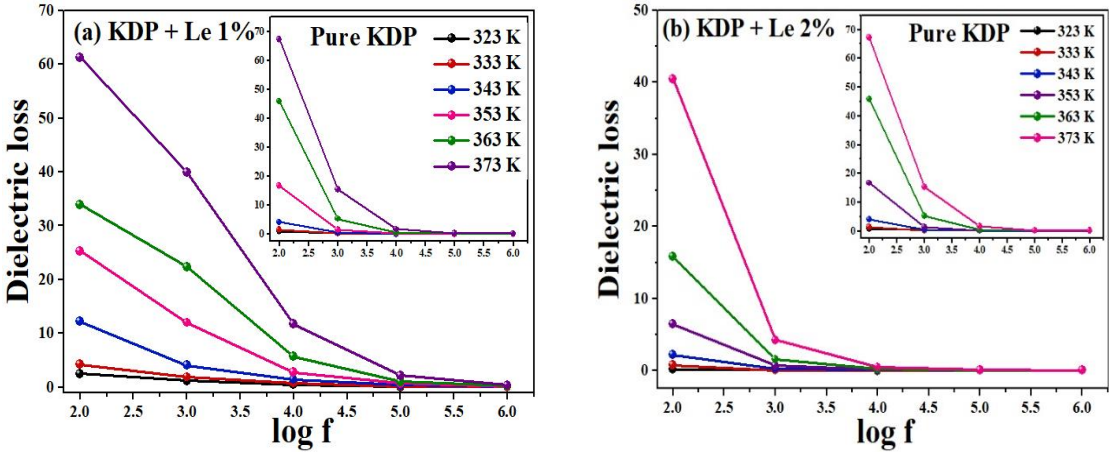

Figures 4. (a) Variation of dielectric loss with the frequency of L-Leucine (1 mol%) doped KDP crystal and **(b)** Variation of dielectric loss with the frequency of L-Leucine (2 mol%) doped KDP crystal.

3.2.1 Impedance Spectroscopy:

Figures 5(a-c) shows Nyquist plots [real part of complex impedance (Z') against imaginary part of complex impedance (Z'')] of pure and L-Leucine (1 mol% and 2 mol%) doped KDP crystals. A complex plane impedance plot represents the electrical characteristics of a sample. Intragrain, intergrain and electrode processes are the most common causes that influence the impedance characteristics. There are many ways by which the motion of charges can be described. These include dipole re-orientation, space charge formation and charge displacement. At each temperature, a single semi-circular arc is seen. Due to the presence of temperature-dependent multi-relaxation processes, the centre of each semi-circle lies below the real axis (Z').

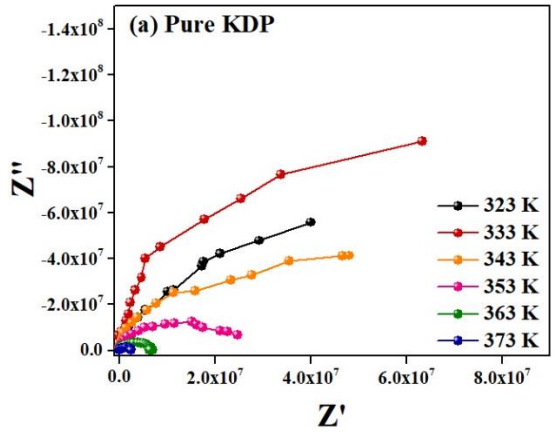

Figure 5(a). Nyquist plot of pure KDP crystal

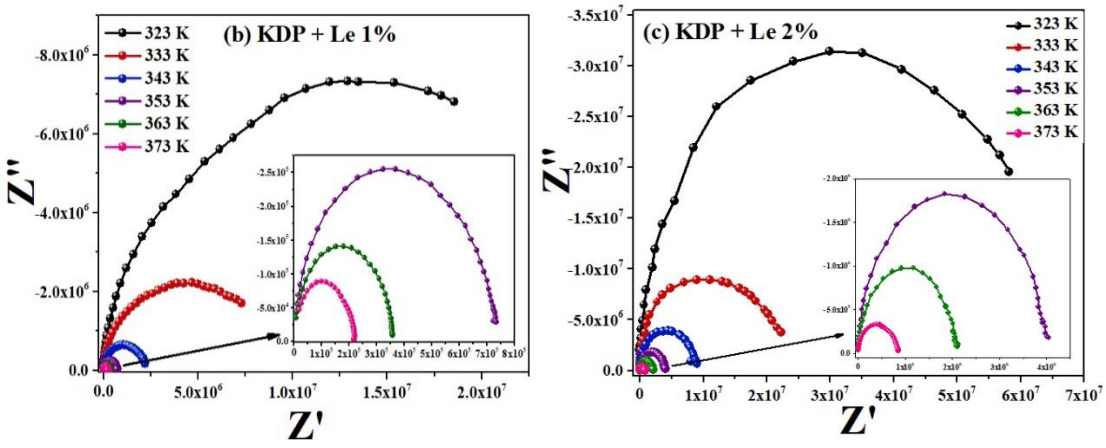

Figures 5. (b) Nyquist plot of L-Leucine (1 mol%) doped KDP crystal and **(c)** Nyquist plot of L-Leucine (2 mol%) doped KDP crystal

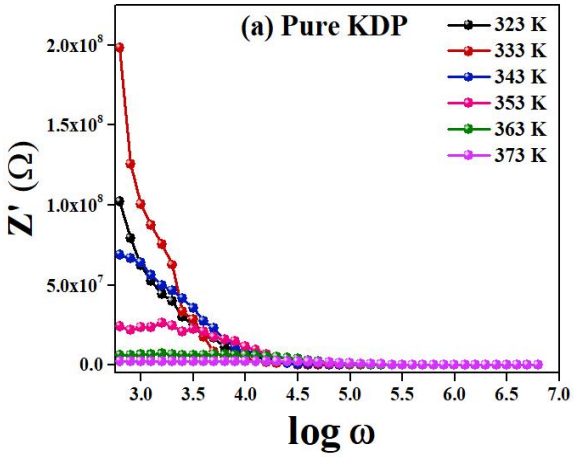

Figure 6(a). Variation of the real part of impedance (Z') with frequency for pure KDP crystal

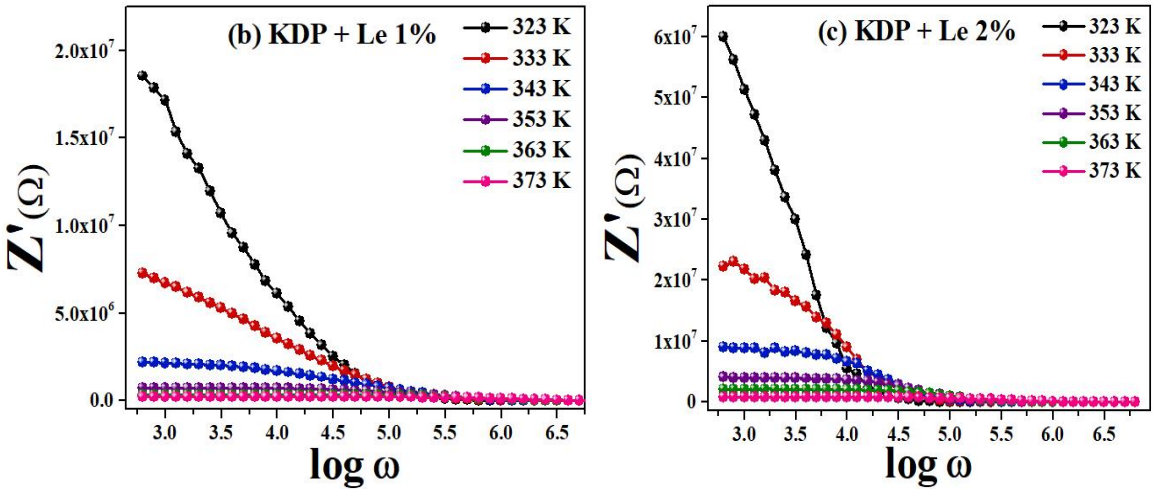

Figures 6. (b) Variation of the real part of impedance (Z') with frequency for L-Leucine (1 mol%) doped KDP crystal and **(c)** Variation of the real part of impedance (Z') with frequency for L-Leucine (2 mol%) doped KDP crystal

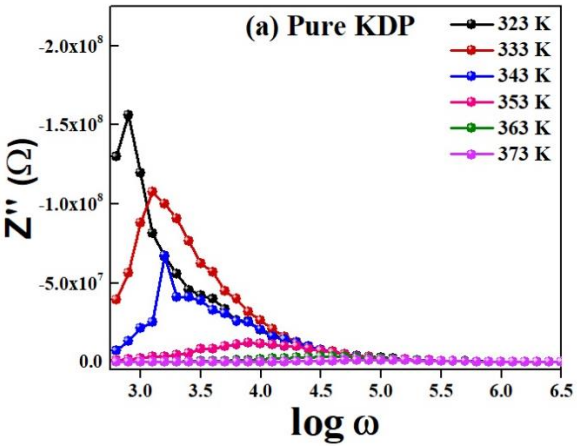

Figure 6(d). Variation in the imaginary part of impedance (Z'') with frequency for pure KDP crystal

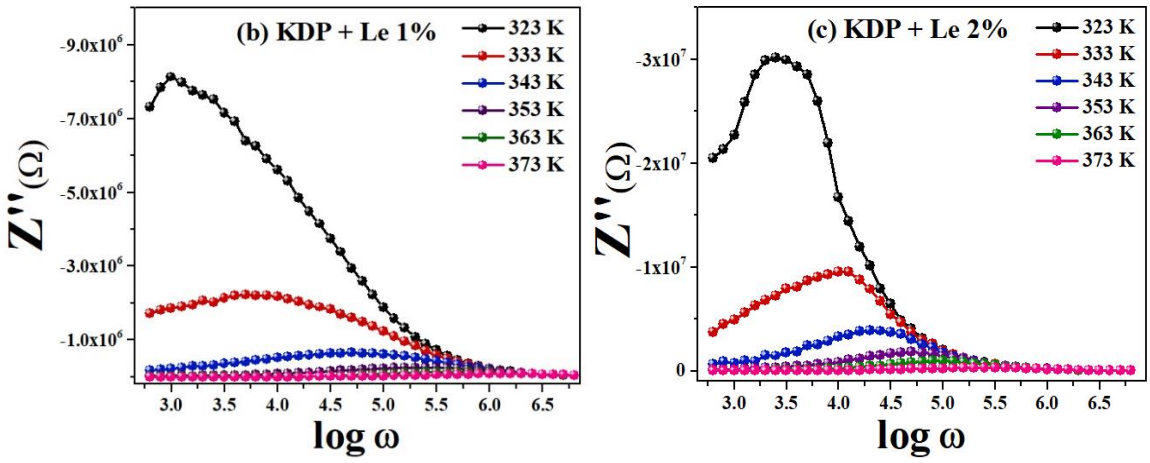

Figures 6. (e) Variation in the imaginary part of impedance (Z'') with frequency for L-Leucine (1 mol%) KDP crystal and **(f)** Variation in the imaginary part of impedance (Z'') with frequency for L-Leucine (2 mol%) KDP crystal

This indicates that the crystals display non-Debye behaviour. A tail (or spike) can be seen at lower frequencies. This might be due to the polarisation of the electrode/electrolyte. The values of bulk resistance, relaxation time and capacitance were calculated and are presented in table 3, obtained with fitting the semi-circles of the Nyquist plot. The reduced concentration of oxygen vacancies and other charge carriers (e.g., trapped electrons and holes) in the grain boundaries accounts for the high bulk resistance at all temperatures.

The dependences of the real part (Z') and imaginary part (Z'') of the impedance on the frequency at various temperatures are shown in figures 6(a-f). The value of Z' decreases as the temperature and frequency increase, indicating that the crystals have a negative temperature coefficient of resistance (NTCR). The loss spectrum, as shown in figures 6 (d-f), is characterized by many key characteristics, including the appearance of a peak (max Z''_{max}), asymmetric peak broadening and a reduction in values of Z''_{max} that shift to higher temperatures as frequency increases. The asymmetric broadening of peaks in frequency explicit plots of Z'' indicates a range of relaxation periods, implying that the material exhibits a temperature-dependent electrical relaxation phenomenon.

Table 3. Nyquist parameters of pure and L-Leucine doped KDP crystals

Temperature	KDP			KDP + Le 1%			KDP + Le 2%		
	R_g (Ω)	C_g (pF)	τ (μs)	R_g (Ω)	C_g (pF)	τ (μs)	R_g (Ω)	C_g (pF)	τ (μs)
323 K	1.17E+09	10.812	1.2642	1.13E+07	88.83	1004.71	6.08E+07	6.5835	399.98
333 K	3.36E+08	2.374	0.7980	4.06E+06	49.33	200.46	1.93E+07	5.2013	100.47
343 K	7.65E+07	8.283	0.6339	1.53E+06	13.12	20.04	7.94E+06	6.3427	50.35
353 K	2.61E+07	4.848	0.1264	6.21E+05	6.438	3.99	3.86E+06	5.1894	20.04
363 K	7.06E+06	4.502	0.0317	3.75E+05	5.373	2.00	2.08E+06	6.0813	12.64
373 K	2.50E+06	3.990	0.0100	2.01E+05	3.156	0.63	7.68E+05	5.2067	3.99

3.2.2 A. C Conductivity Mechanism:

Figures 7(a-c) depict the relationship between electrical A. C conductivity and angular frequency of the crystals at temperatures ranging from 323 K to 373 K. Conductivity has a frequency-independent characteristic in the low-frequency region, which is referred to as the DC component of conductivity. Funke's jump relaxation model (JRM) has been used to explain frequency-independent D. C conductivity [23]. The hopping frequency is the rate at which frequency independent phenomena become dependent. With increasing temperature, the low frequency plateau region in the conductivity spectra shifts to higher frequencies. The high frequency conductivity shows dispersion, which could be attributed to the rapid increase in charge carrier mobility. A detailed discussion on the increase of A. C conductivity with frequency has already been given in chapter-4.

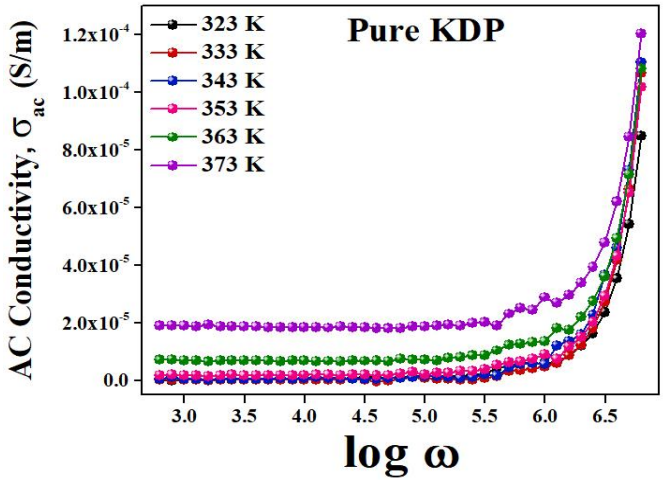

Figure 7(a). A. C Conductivity of pure KDP crystal

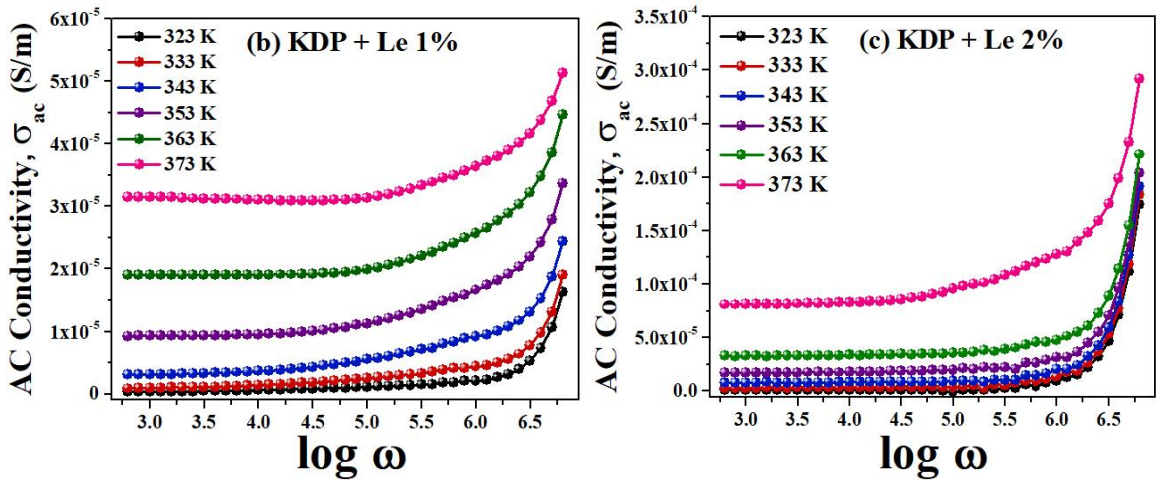

Figures 7. (b) A. C Conductivity of L-Leucine (1 mol%) doped KDP crystal and **(c)** A. C Conductivity of L-Leucine (2 mol%) doped KDP crystal

3.2.3 Jonscher's Plots:

Jonscher's proposed double power law [24] can be used to calculate total conductivity at a given temperature. The electrical response of a material's power law dispersion has been understood as a network of resistors and capacitors, leading to the expression [25].

$$\sigma'_{ac}(\omega) = \sigma_0 + A\omega^s \quad (1)$$

where ω = 2πf is the angular frequency of the applied voltage, σ_0 = D. C conductivity, A is constant, s is material's property which can have values between 0 to 1.

Jonscher plots for pure and L-Leucine doped KDP crystals are shown in figures 8 (a-c), which exhibit extremely dispersive behaviour due to the existence of just a. c conductivity. At all temperatures, the values of the exponent 's' and σ_0 are found by fitting equation (1). Table 4 shows that the value of dc conductivity increases with increasing temperature and dopant concentration. Table 5 shows that for pure, L-Leucine (1 mol% and 2 mol%) doped KDP crystals, the 's' parameter value decreases linearly with temperature. Here, the correlated barrier hopping (CBH) model is an acceptable model to represent the phenomena since the nature of the plot indicates a decreasing trend of the exponent 's' with an increase in temperature [26]. As a result, the most likely conduction mechanism for the crystals, according to the CBH model, is the classical hopping of charge carriers between localized sites over the potential barrier.

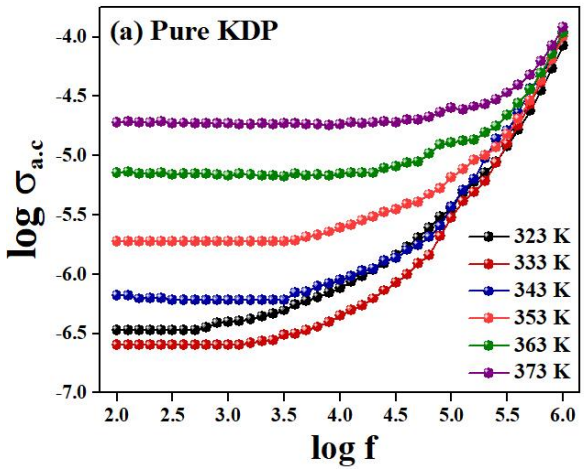

Figure 8(a). Jonscher's plot of pure KDP crystal

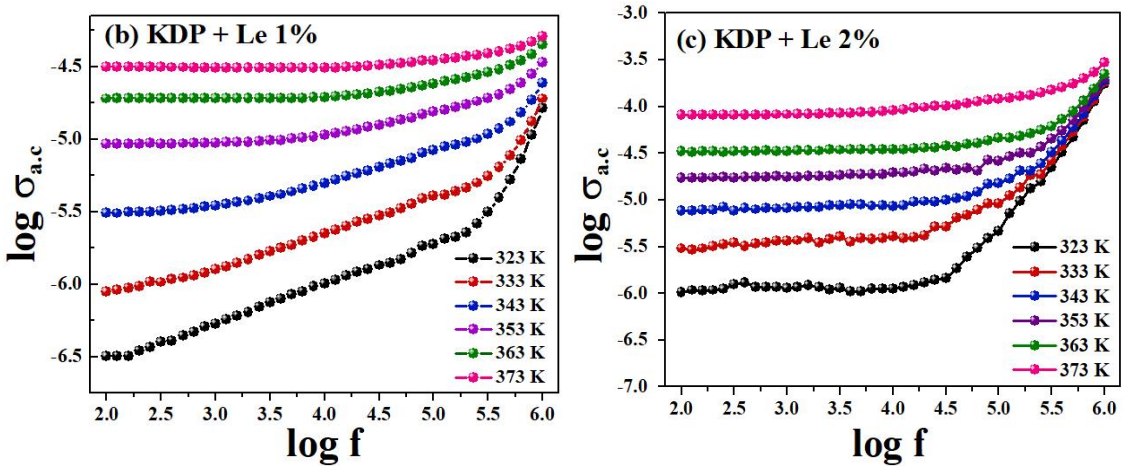

Figures 8. (b) Jonscher's plot of L-Leucine (1 mol%) doped KDP crystal and **(c)** Jonscher's plot of L-Leucine (2 mol%) doped KDP crystal

Table 4. σ_{dc} conductivity values of pure and L-Leucine (1 mol% and 2 mol%) doped KDP crystals

Temperature	$\sigma_{d.c}$ conductivity		
	Pure KDP	**KDP + Le 1%**	**KDP + Le 2%**
323 K	0.8901×10^{-7}	0.2735×10^{-6}	0.105×10^{-5}
333 K	0.92×10^{-7}	0.804×10^{-6}	0.2952×10^{-5}
343 K	5.854×10^{-7}	2.95×10^{-6}	0.8153×10^{-5}
353 K	1.8236×10^{-6}	0.915×10^{-5}	1.6854×10^{-5}
363 K	0.7×10^{-5}	1.885×10^{-5}	3.327×10^{-5}
373 K	1.8855×10^{-5}	3.125×10^{-5}	7.985×10^{-5}

Table 5. Jonscher's plot parameters for pure and L-Leucine (1 mol% and 2 mol%) doped KDP crystal

Temperature	A ($s.m^{-1}.rad^{-n}$)			s - parameter		
	Pure KDP	KDP+Le 1%	KDP+Le 2%	Pure KDP	KDP+Le 1%	KDP+Le 2%
323 K	0.325×10^{-8}	0.3582×10^{-8}	0.07587×10^{-9}	0.6252	0.5864	0.9782
333 K	0.3369×10^{-8}	0.8251×10^{-8}	0.1547×10^{-8}	0.6021	0.5637	0.7368
343 K	0.3519×10^{-8}	1.268×10^{-8}	0.2571×10^{-8}	0.5821	0.5402	0.6975
353 K	0.4021×10^{-8}	1.376×10^{-8}	0.3587×10^{-8}	0.5624	0.5336	0.6852
363 K	0.5023×10^{-8}	1.4213×10^{-8}	0.4285×10^{-8}	0.5325	0.5268	0.6723
373 K	0.543×10^{-8}	1.4632×10^{-8}	2.225×10^{-8}	0.5089	0.5021	0.6612

The binding energies (W_m) of the crystals grown the density of states at the Fermi level and activation energy were calculated with the help of the formulae (Ref: Chapter-4). The binding energy W_m was calculated from the slope of the linear plot of 1-s against T. Figure 9 depicts the change of 1-s with temperature for pure and L-Leucine doped KDP crystals. The binding energies of pure KDP, L-Leucine (1 mol%) doped KDP and L-Leucine (2 mol%) doped KDP crystal are found to be 0.2238 eV, 0.335 eV and 0.3541 eV.

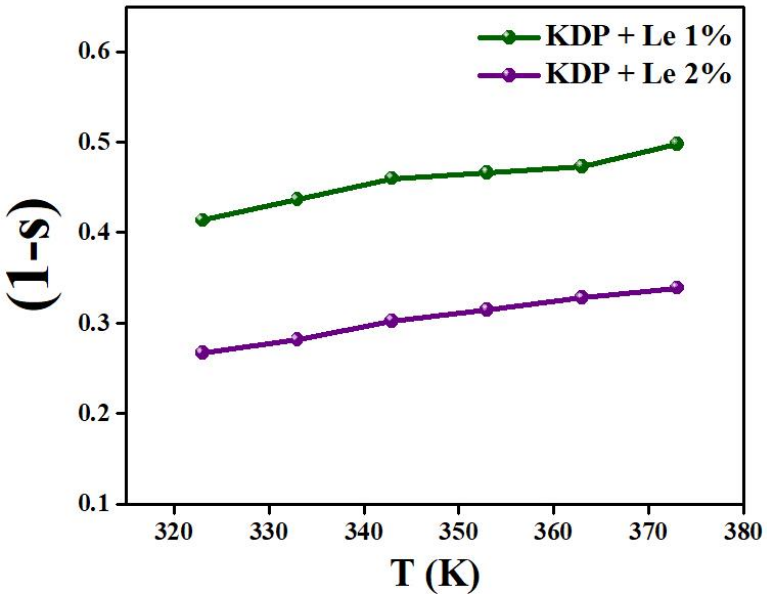

Figure 9. Binding energy plot of pure and L-Leucine (1 mol % and 2 mol%) doped KDP crystals

Figures 10 (a-c) depict the variation of density of states at the Fermi level $[N(E_f)]$ with frequency. The density of states $[N(E_f)]$ of pure KDP and L-Leucine doped KDP crystals decreases with increasing frequency. The value of $N(E_f)$ initially drops to a minimum for a

given temperature range, which agrees with the dielectric constant and A. C conductivity results.

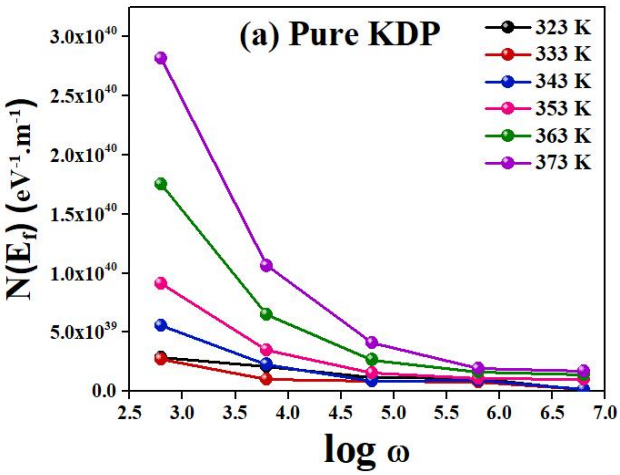

Figure 10(a). The variation of density of states at the Fermi level with frequency for pure KDP crystal

As a result, both frequency and temperature can influence the system's electrical conductivity at low frequencies. In contrast, charge carriers are carried to localized sites by thermal agitation at higher frequencies. The relatively large values of $N(E_f)$ (~10^{39} – 10^{40}) imply that charge transport in the crystals is dominated by hopping between pairs of sites.

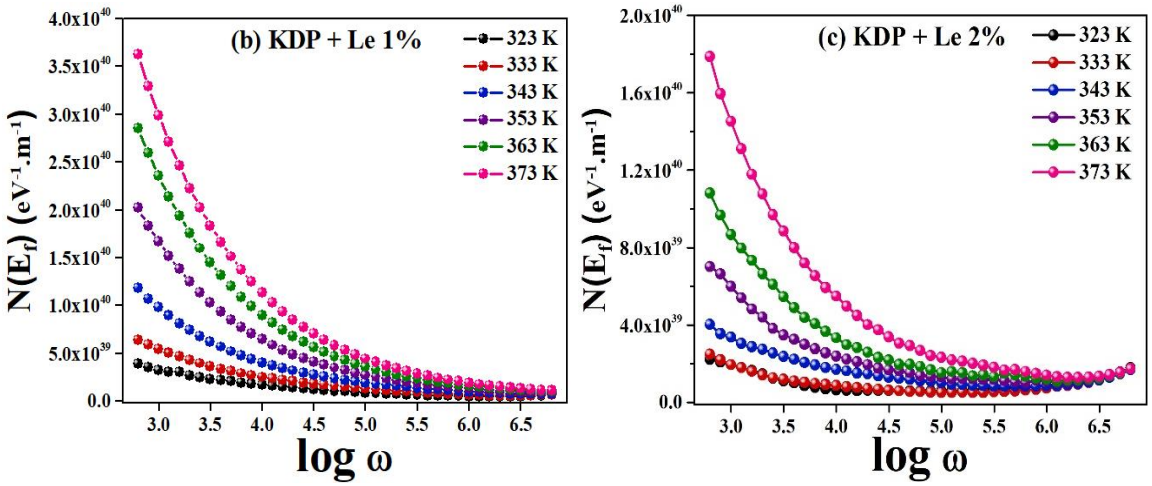

Figures 10. (b) The variation of density of states at the Fermi level with frequency for L-Leucine (1 mol%) doped KDP crystal and **(c)** The variation of density of states at the Fermi level with frequency for L-Leucine (2 mol%) doped KDP crystal

Figures 11 (a-c) show the $\log_{a.c}$ versus 1000/T variation for pure and L-Leucine doped KDP crystals at various frequencies. The slopes of linear fitted curves of $\log_{a.c}$ vs 1000/T were used to determine the activation energies of pure and L-Leucine doped KDP crystals. The

activation energies obtained at different frequencies are listed in table 6. Table 6 indicates that as the frequency increases, the activation energies of pure KDP and L-Leucine (1 mol% and 2 mol%) doped KDP crystals decrease, suggesting that electronic charge carriers may hop between various localized states in the material [27].

Table 6. The calculated values of activation energies of pure and L-Leucine (1 mol% and 2 mol%) doped KDP crystals

Frequency	Activation Energy (Ea) (eV)		
	Pure KDP	KDP + Le 1%	KDP + Le 2%
100	1.2382	0.2473	0.0580
1000	1.1775	0.5943	0.0619
10000	1.1300	0.7036	0.8338
100000	0.7133	0.8499	0.8441
1000000	0.0310	0.96041	0.8594

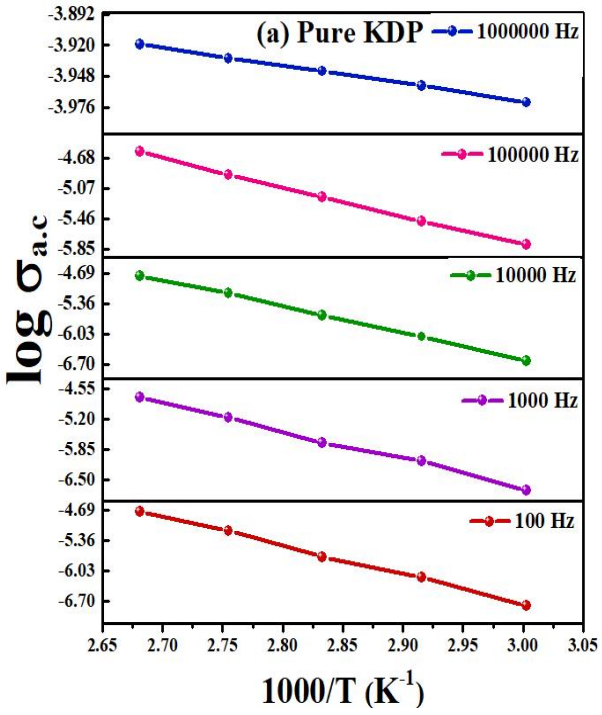

Figure 11(a). Activation energies plot for pure KDP crystal

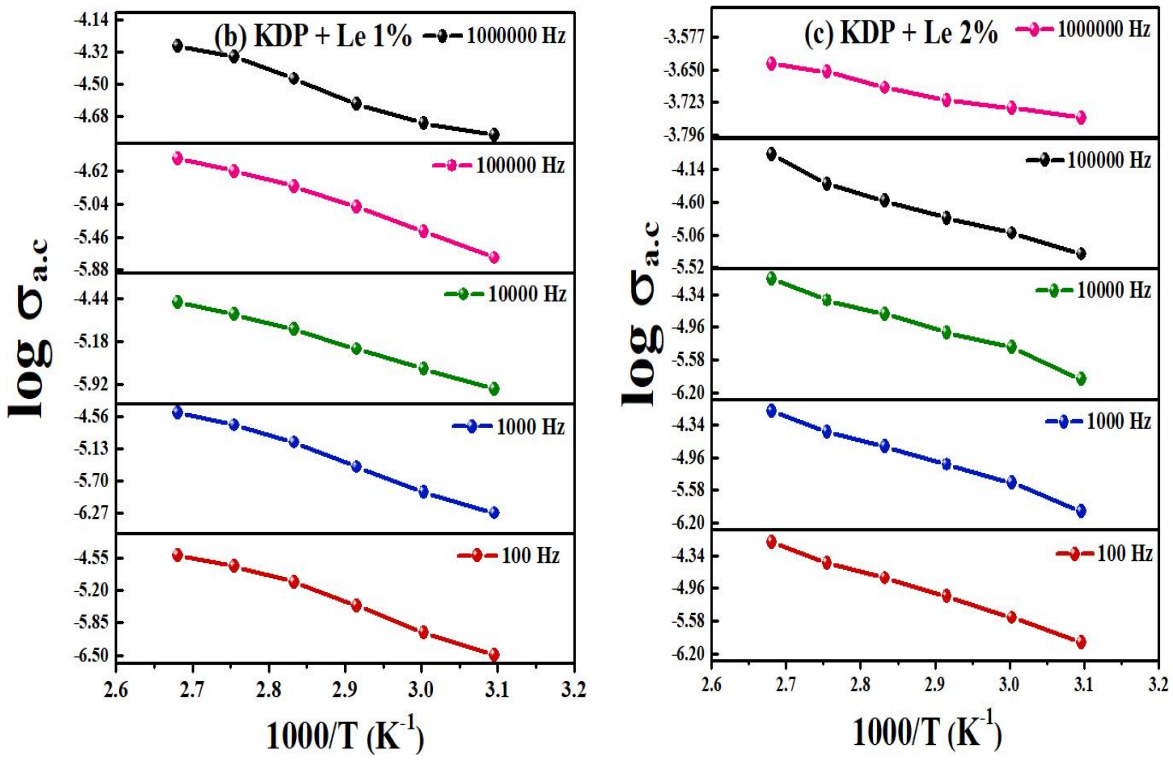

Figures 11. (b) Activation energies plot for L-Leucine (1 mol%) doped KDP crystal and **(c)** Activation energies plot for L-Leucine (2 mol%) doped KDP crystal

3.2.4 Complex Modulus Spectroscopy:

Complex modulus spectroscopy is an essential analytical technique because it can distinguish electrode polarisation from grain boundary conduction processes involved in electrical relaxation. The formula for calculating complex modulus is already described in Chapter-4. Figures 12 (a-c) show that variation of the imaginary part of complex modulus (M'') with the real part of complex modulus (M') in the temperature range of 323 K - 373 K. As seen in figures 12(a-c), all semi-circles whose centres do not lie on the real axis are represented by one semi-circle, implying non-Debye type relaxation inside crystals.

Figures 13(a-c) and figures 14(a-c) show how the real part (M') and the imaginary part (M'') of the complex modulus vary with angular frequency at temperatures ranging from 323 K to 373 K. From figures 13(a-c), we observe that M' has a lower magnitude at lower frequencies and displays continuous dispersion as frequency increases.

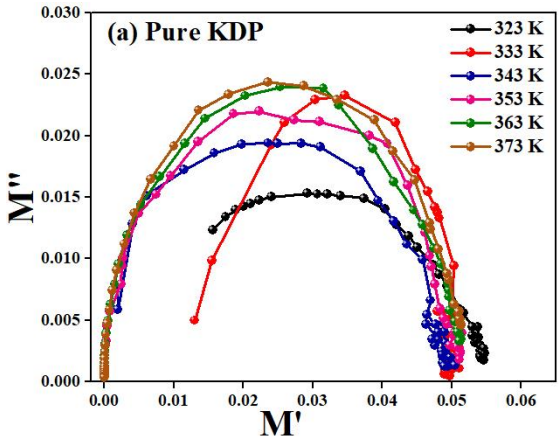

Figure 12(a). Variation in real (M') and imaginary (M'') parts of complex modulus for pure KDP crystal

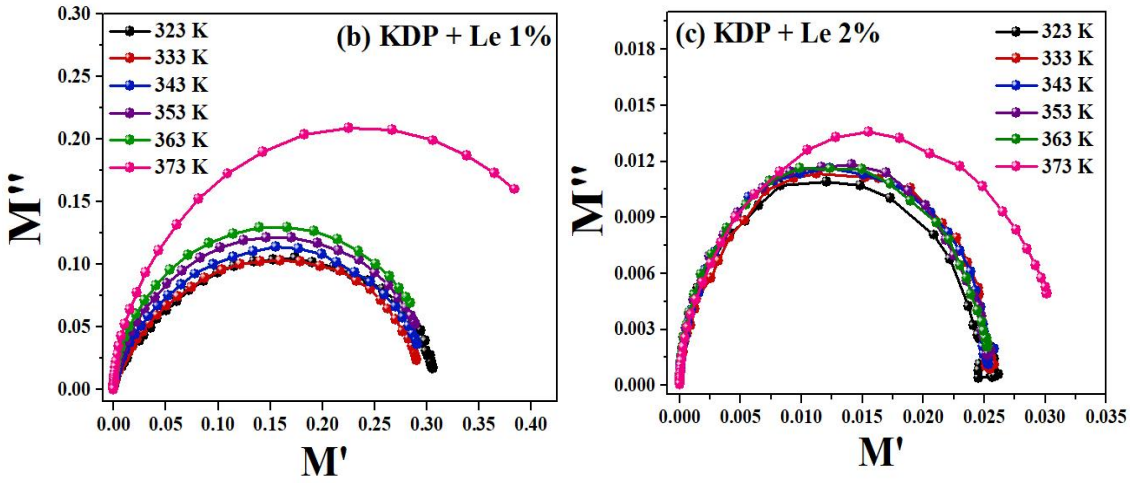

Figures 12. (b) Variation in real (M') and imaginary (M'') parts of complex modulus for L-Leucine (1 mol%) doped KDP crystal and **(c)** Variation in real (M') and imaginary (M'') parts of complex

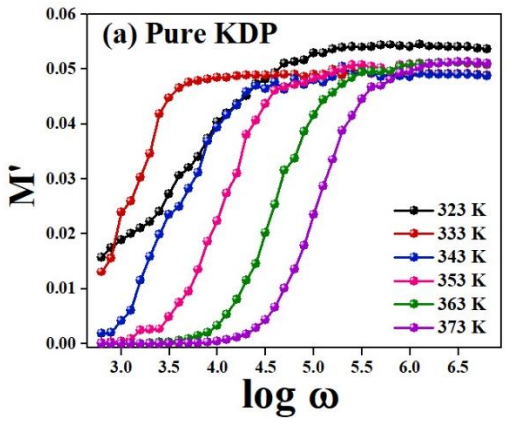

Figure 13(a). Variation of the real part of complex modulus (M') with angular frequency for pure KDP crystal

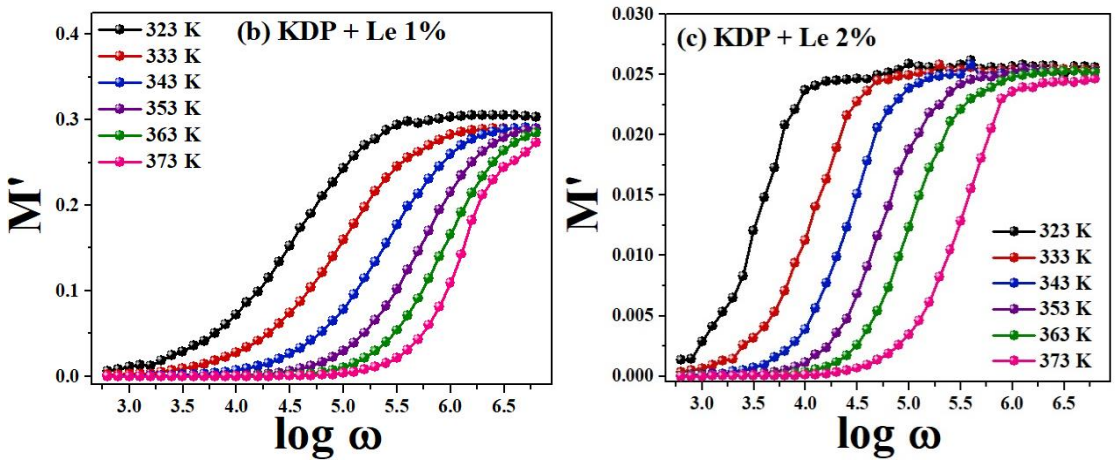

Figures 13. (b) Variation of the real part of complex modulus (M') with angular frequency for L-Leucine (1 mol%) doped KDP crystal and **(c)** Variation of the real part of complex modulus (M') with angular frequency for L-Leucine (2 mol%) doped KDP crystal

With increasing temperature, the maxima peaks M''_{max} shift toward the high frequency side. For all of the given temperatures, a sigmoidal reduction in the value of M' is seen with increasing frequency, owing to the long-range mobility of charge carriers under the action of an induced electric field. The increase in peak height in the M'' versus log ω plot is due to a decrease in capacitance as temperature increases, one of the most major properties of a ferroelectric material above the ferroelectric-paraelectric phase transition temperature T_c. The region where the carrier can migrate over long distances is defined by the frequency range below the relaxation peak in the imaginary part of the modulus M''. Because of the difference in a number of charge carriers, the modulus spectrum shows that a hopping process exists, contributing significantly to electrical conductivity at high temperatures.

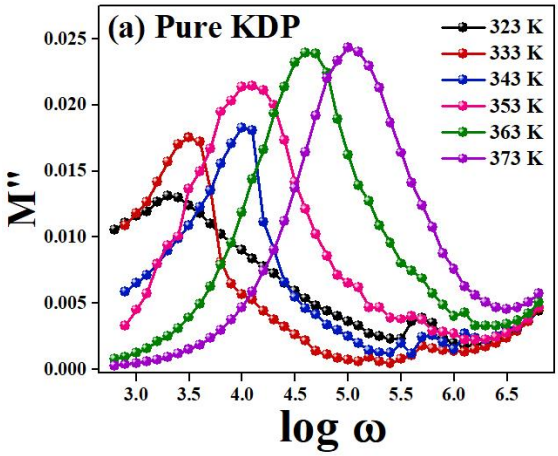

Figure 14(a). Variation of the imaginary part of complex modulus (M'') with angular frequency for pure KDP crystal

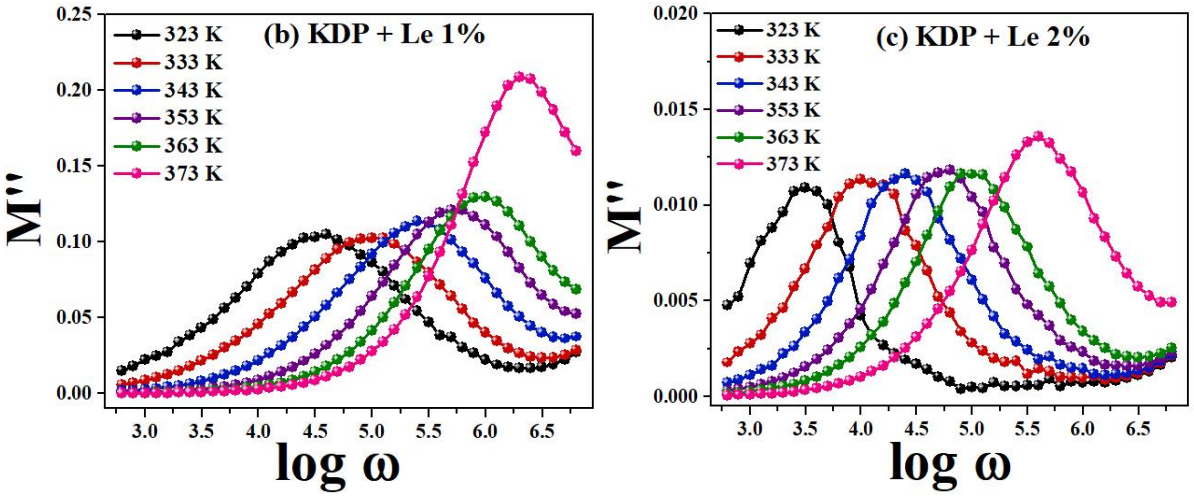

Figures 14. (b) Variation of the imaginary part of complex modulus (M'') with angular frequency for L-Leucine (1 mol%) doped KDP crystal and **(c)** Variation of the imaginary part of complex modulus (M'') with angular frequency for L-Leucine (2 mol%) doped KDP crystal

It is observed that there is at least one relaxation peak at each temperature. With the help of relaxation peaks at different temperatures, the stretch exponent parameter (β) was calculated and is summarized in table 7. In both pure and L-Leucine doped KDP crystals, the value of β deviates from unity, indicating the presence of a non-Debye type relaxation mechanism.

Table 7. The calculated values of stretch exponent parameter (β) for pure KDP and L-Leucine (1 mol% and 2 mol%) doped KDP crystals

Temperature	Stretch exponent parameter (β)		
	Pure KDP	KDP + Le 1%	KDP + Le 2%
323	0.5568	0.7270	0.9624
333	0.9104	0.6886	0.9719
343	0.9245	0.6474	0.9818
353	0.9363	0.6794	0.9528
363	0.9628	0.7233	0.9048
373	0.9237	0.6788	0.7215

3.3 Fourier Transform Infrared (FT-IR) Spectroscopy:

Figure 15 show the FTIR spectra of pure and L-Leucine (1 mol% and 2 mol%) doped KDP crystals. Due to the O–H stretching vibrations in KDP and water, broadband is observed in the higher energy region of the KDP spectrum. This broadening is mainly caused by

hydrogen bonding within the crystal. The corresponding modes and functional groups of pure and L-Leucine doped KDP crystals are listed in table 8. Due to the overlapping of some amino acid vibrations on KDP bands, some frequencies are observed to have shifted, and as a result, some bands in the KDP spectrum have broadened. The absorption corresponding to NH stretching and C-N-H stretchings are present in doped KDP crystals compared to pure KDP crystals, indicating that L-Leucine got successfully doped in KDP.

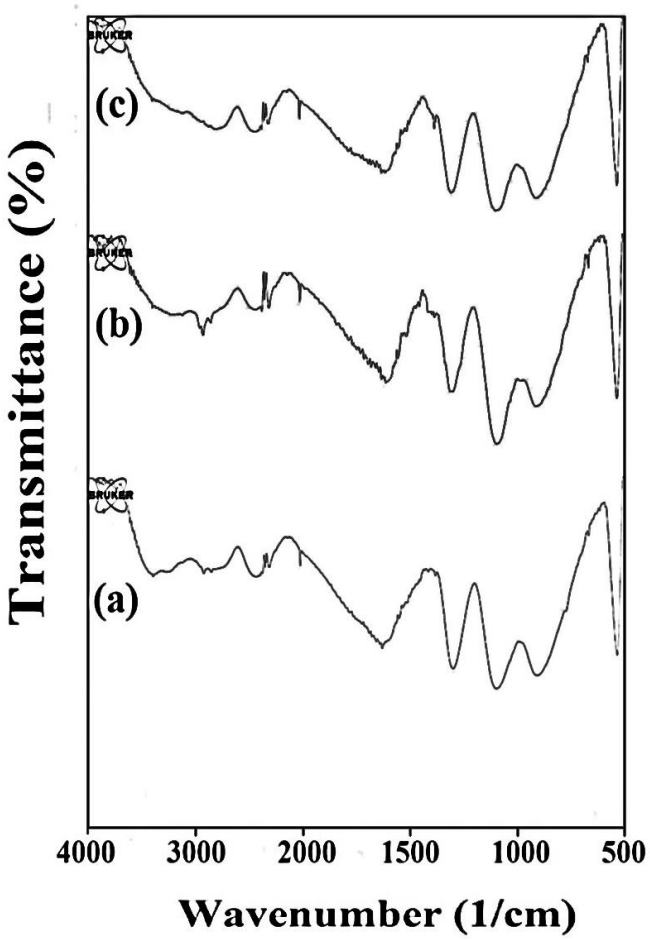

Figure 15. (a) FT-IT spectrum of pure KDP, **(b)** FT-IR spectrum of L-Leucine (1 mol%) doped KDP crystal and **(c)** FT-IR spectrum of L-Leucine (2 mol%) doped KDP crystal

The NH^{3+} stretching vibrations of amino acids (2700-3300cm^{-1}) coincide with the KDP's OH stretching vibrations. In the spectra of L-Leucine doped KDP crystals, symmetric stretchings of C–H, C=O and COOH groups are observed. By combining an unoccupied H-vacancy with the hydrogen atom of KDP, the dopant L-Leucine is expected to form L-defects. As a result, hydrogen's fundamental vibration is rehabilitated. The force constant of O-H vibration of pure and L-Leucine is calculated and summarized in table 9 (The formula of force constant is already described in chapter-4). According to the calculated values of the force

constant of O-H vibrations, the inclusion of L-Leucine in the KPD lattice induces reformation in force constant values.

Table 8. Functional groups of pure and L-Leucine (1 mol% and 2 mol%) doped KDP crystals

Bond Assignments	**Wavenumber (cm^{-1})**		
	Pure KDP	**KDP + Le 1%**	**KDP + Le 2%**
O-H vibration	3321	3323	3325
NH_3 asymmetric stretching	-	3398	3393
N-H stretching	-	2921	2931
O-H asymmetric stretching	2927	2925	2921
O-P-OH symmetric stretching	1704	1678	1678
N-C-N stretching	-	1680	1690
O-H bending	1630	1631	1631
O=P-OH stretch	1614-1695	1631	1631-1678
O=P-OH stretching	1652	1659	1657
NH_3 bending	-	1453	1452
P-O-H bending	1448	1453	1452
C-COO^- symmetric stretching	-	1415	1416
C-N-H stretching	-	1302	1306
P=O stretching	1295	1096	1099
P-O-H stretching	909	912	908
COOH rocking	-	677	677
COO^- bending	-	617-668	616-669
NH_2 bending	-	536	533

Table 9. The calculated values of Force Constant of O-H vibration of pure and L-Leucine doped KDP crystal

Sample	**Absorption Wavenumber (cm^{-1})**	**Force Constant (Nm^{-1})**
Pure KDP	3321	591.14
KDP + Le 1%	3398	591.18
KDP + Le 2%	3397	592.57

3.4 Ultraviolet-Visible (UV-Vis) Spectroscopy:

A good optical transmittance is desirable in an NLO (Non-Linear Optical) crystal since absorption near the fundamental of the second harmonic of an Nd: YAG laser will lead to a loss of SHG (Second Harmonic Generation) efficiency. This has been a specific drawback in many organic crystals [1]. Optically transparent crystals in the UV-Visible wavelength region hold good for optical applications, especially for SHG (Second Harmonic Generation). Crystals having the lowest absorption and wider transparency are naturally most favoured for developing optoelectronic and NLO devices. We can say that the crystals show very good transparency in the entire visible region from the transmittance spectra. There is no significant absorption in the range of 200-800 nm. As there is no absorption, the crystal is found to be transparent in the visible and near IR region, an essential characteristic required for the frequency doubling process [2]. This is an advantage of using amino acids where the absence of strongly conjugated bonds leads to a wider transparency range in the visible and UV spectral region [3].

The formulae for optical absorption coefficient (α), optical energy band gap, refractive index (η), extinction coefficient (K), skin depth (δ), and optical conductivity have been already discussed in Chapter-4. From figure 16, it is observed that the cut-off wavelengths of pure KDP and L-Leucine doped KDP (1 mol% & 2 mol%) are 245 nm, 238 nm and 236 nm, respectively. The Tauc plot of $(\alpha h\upsilon)^2$ versus E for pure and doped KDP crystals was obtained to find the optical bandgap. The optical band gaps of pure and L-Leucine (1 mol% and 2 mol%) doped KDP crystals were evaluated using extrapolation of the linear part on the high energy side of the spectrum shown in figure 17. The band gaps of pure KDP, L-Leucine doped KDP crystals (1 mol% and 2 mol%) were found to be 3.41 eV, 5.41 eV and 5.57 eV, respectively.

There is enhancement seen in the bandgap with the increase in doping percentage. This significant increase in the bandgap of pure KDP due to amino acid prompts the possibility of increased SHG (Second Harmonic Generation) efficiency. The ability of the dielectric medium (crystal) to be polarized under the influence of strong radiation is demonstrated by crystals with wide bandgaps.

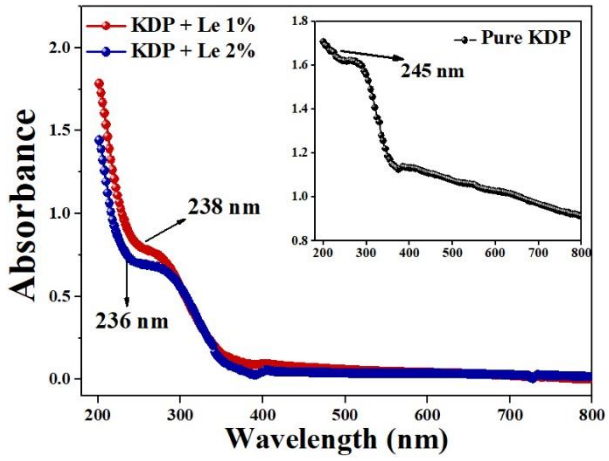

Figure 16. Absorbance spectra for pure and L-Leucine (1 mol% and 2 mol%) doped KDP crystals

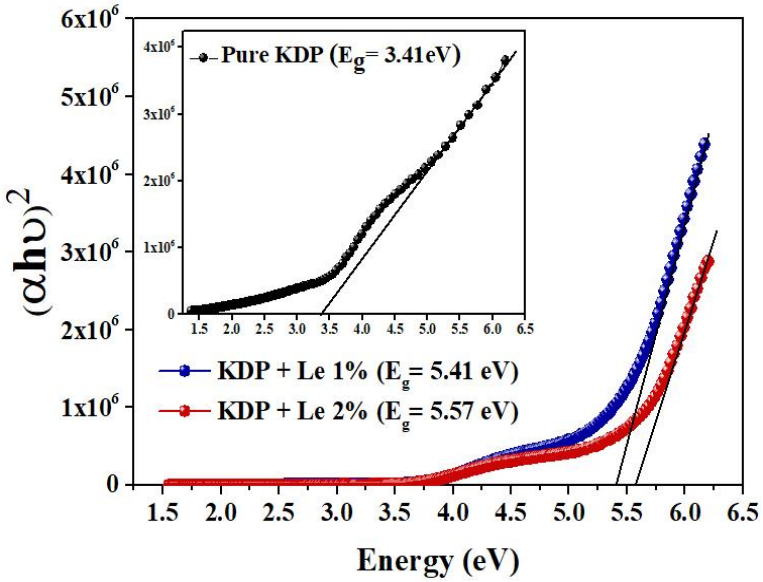

Figure 17. Tauc's plot of pure and L-Leucine (1 mol% and 2 mol%) doped KDP crystal

Figure 18 shows the refractive index variation with wavelength for pure and L-Leucine (1 mol% and 2 mol%) doped KDP crystals. Due to the inclusion of L-Leucine, the refractive index of KDP crystal has enhanced, making doped KDP crystals a very desirable photorefractive material for holographic data storage systems [28].

The response of extinction coefficient to photon energy is shown in figures 19(a-b) for the crystals. Due to the inclusion of L-Leucine, the extinction coefficient of KDP crystal has increased.

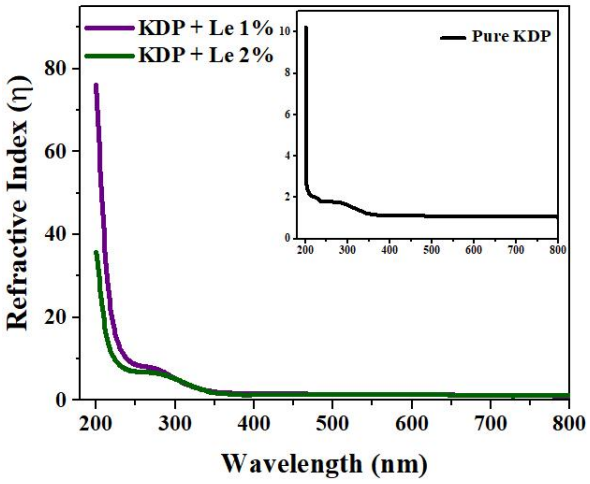

Figure 18. Variation of refractive index with wavelength for pure and L-Leucine (1 mol% and 2 mol%) doped KDP crystals

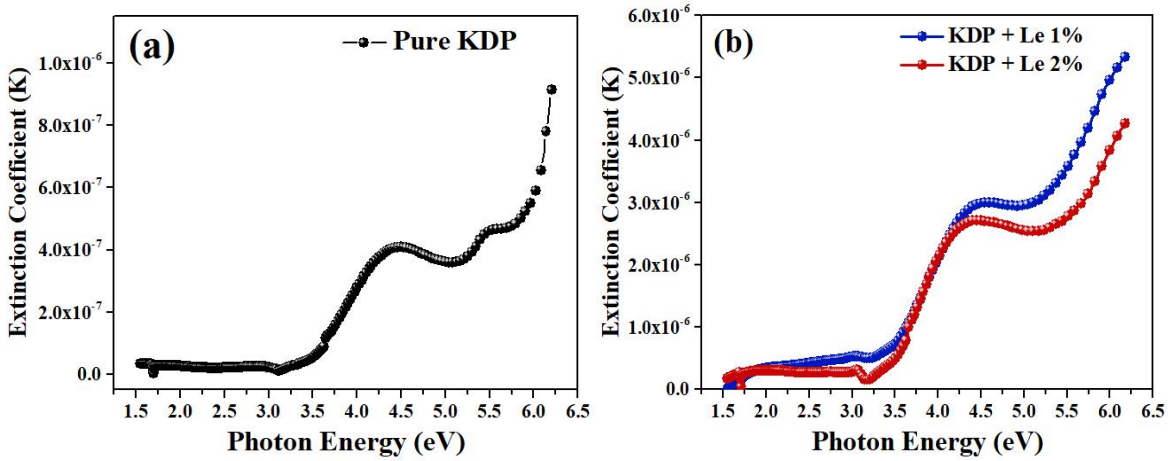

Figures 19. (a) Extinction Coefficient of pure KDP crystal and **(b)** Extinction Coefficient of L-Leucine (1 mol% and 2 mol%) doped KDP crystal

The calculated values of the ordinary and extraordinary refractive indices of KDP are found to be 1.5134 and 1.4672, respectively. Here, the ordinary refractive index is greater than the extraordinary refractive index, which corresponds to the KDP crystal's negative uniaxial aspect and can be utilized in birefringence applications. The variation of optical conductivity with a photon energy of pure and L-Leucine doped KDP crystals is shown in figure 20. It is seen that as the photon energy increases, so does the optical conductivity. Also, as the doping concentration increases, the optical energy increases, implying that the higher the optical conductivity, the higher the conversion efficiency of the crystal.

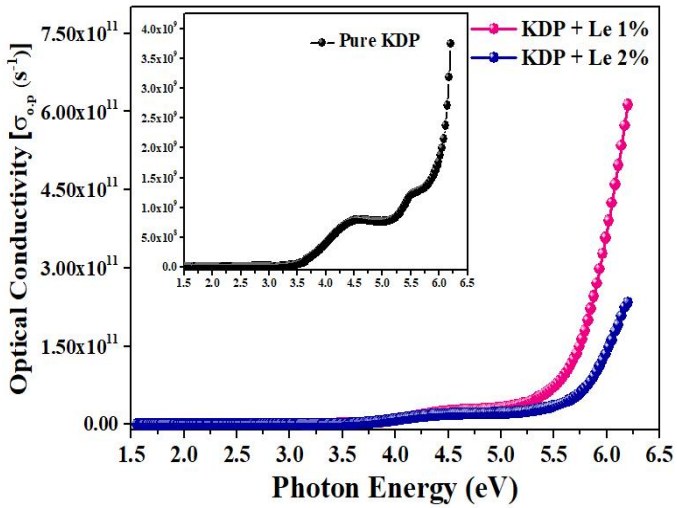

Figure 20. Optical Conductivity of pure and L-Leucine (1 mol% and 2 mol%) doped KDP crystals

3.4.1 Urbach Energy (Absorption band tail):

At the optical band edge, the Urbach tail is the section of the absorption coefficient curve that is exponential. The Urbach empirical rule characterizes the relationship between absorption coefficient and photon energy at the optical bandgap edge. The formula for calculating the Urbach energy is already discussed in chapter-4. The straight-line slope displayed in figure 21 was used to determine the Urbach Energy (E_u) value. The values of E_u were obtained using the plot of ln (α) vs photon energy (eV). Table 10 shows the E_u values that were calculated.

Table 10. The calculated values of Urbach energy (E_u) for pure and L-Leucine (1 mol% and 2 mol%) doped KDP crystals

Sample	Urbach Energy (E_u) (eV)
Pure KDP	0.6391
KDP + Le 1%	0.3038
KDP + Le 2%	0.2952

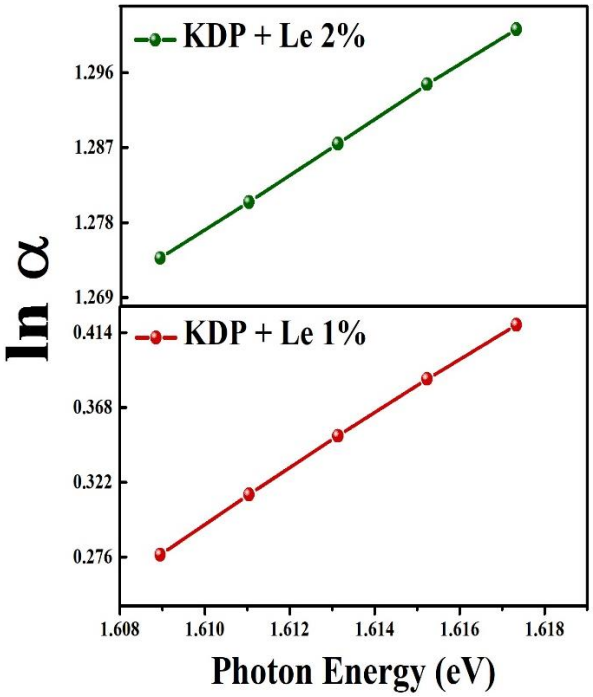

Figure 21. Urbach energy plot for pure and L-Leucine (1 mol% and 2 mol%) doped KDP crystal

3.5 Relative Second Harmonic Generation (SHG) Efficiency:

The intensity of SHG emission indicates the non-linear optical character of the crystals. Green radiation at 532 nm confirms the frequency doubling. SHG requires precise molecular alignment of crystals to facilitate non-linearity in the presence of dopants. The NH^{3+} and COO^{-} groups in L-Leucine are responsible for the enhanced SHG efficiency of L-Leucine doped KDP crystals. Due to these optically active amino groups, there is an increase in non-centro symmetry, boosting SHG efficiency. Here, the introduction of the molecules and the development of extra hydrogen bonds between the molecules and the crystal's expanding face are thought to be responsible for enhancing SHG efficiency. The phosphate group contributes significantly to the efficiency of second harmonic generation (SHG) in KDP, and its exceptional third-order non-linear optical (TONLO) characteristics emphasize its relevance for optical switching devices [29,30]. Table 11 indicates the values of relative SHG efficiency of pure and L-Leucine doped KDP crystals.

Table 11. Relative SHG efficiency of pure and L-Leucine (1 mol% and 2 mol%) doped KDP crystals

Sample	Relative SHG Efficiency
Pure KDP	-
KDP + Le 1%	1.5
KDP + Le 2%	2.5

4. Conclusion:

Using the slow evaporation growth technique at room temperature, good quality crystals of pure and L-Leucine (1 mol% and 2 mol%) doped KDP crystals were successfully grown. By doping L-Leucine amino acid into the KDP crystal, its optical and dielectric characteristics are found to enhance usefully for its applicability in various NLO device applications. The tetragonal structure and minor changes in lattice parameters of doped KDP crystals were verified with XRD analysis. Due to the inability of electric dipoles to comply with the applied field and lattice defect developed within crystals, the dielectric constant and dielectric loss decreases with applied angular frequency for all crystals. The a. c conductivity of KDP crystals doped with the amino acid L-Leucine is observed to have enhanced due to the generation of lattice defects. With the help of Jonscher's power law, it is observed that pure and L-Leucine doped KDP crystals follow the Correlation Barrier Hopping (CBH) conduction mechanism. The values of binding energy (W_m) and density of states at Fermi level [$N(E_f)$] were calculated. For all the crystals, the a. c conductivity behaviour signifies a thermally induced mechanism. The Nyquist plots reveal one depressed semi-circle for all crystals investigated, successfully represented by one R-CPE parallel circuit. Complex impedance spectroscopy analysis shows that even a small amount of L-Leucine doping in KDP crystal causes significant changes in the bulk resistance and capacitance values and the conduction mechanism. The presence of amino acid functional groups in the doped KDP spectra confirms the inclusion of L-Leucine in the KDP lattice. L-Leucine doping causes minor structural changes in the KDP crystalline matrix, as seen by slight shifts in vibrational frequencies in FT-IR spectra of doped KDP crystals. Due to the addition of L-Leucine (1 mol% and 2 mol%), the optical transmittance of pure KDP crystal is increased by 2% and 3%, respectively. It is observed that the bandgaps of L-Leucine (1 mol% and 2 mol%) doped KDP crystals are more than that of the pure KDP crystal. The results indicate that the materials may prove good for use in optical devices. L-Leucine (1 mol% and 2 mol%) doping successfully adjusts the

transmittance cut-off, extinction coefficient and refractive index of KDP crystal in the visible region, which is important for UV-tunable lasers, holographic data storage and photonic devices. The presence of a very high photoresponsive nature of the material is confirmed by the large magnitude of optical conductivity (10^{11} s^{-1}). The low values of Urbach energy (E_u) suggest that crystals have high crystalline perfection. The L-Leucine doped crystals' SHG conversion efficiency is higher than that of the pure KDP crystal and is improved with increasing doping concentration. These investigations imply that L-Leucine doping significantly improves crystalline perfection, SHG efficiency and optical transparency, with a considerable correlation between crystalline perfection, optical transparency and SHG.

References:

1. Y. Velikov, I. Pritula, I. Ganina, et al., *Cryst. Res. Technol.*, **42** (2007) pp. 27-33.
2. J. P. Lindl, *Phys. Plasmas*, **2** (1995) pp. 3933-4024.
3. D. Eilmerl, *Ferroelectrics*, **72** (1987) pp. 95-139.
4. P. Selvarajan, J. Glorium Arul Raj, S. Peruaml, *J. Cryst. Growth*, **311**(15) (2009) pp. 3835-3840.
5. P. Kumaresan, S. Moorthy Babu, P. M. Anbarasan, *Opt. Mater.*, **30** (2008) pp. 1361-1368.
6. G. W. Lu, H. R. Xia, et al., *J. Cryst. Growth,* **233** (2001) pp. 730-736.
7. R. W. G. Wyckoff (2nd Ed.), *"Crystal Structure"*, 3, Interscience, New York (1960).
8. P. Gandhimathi, J. Shanthi, *Int. Jr. of Engg. Res. and Techno*., **2**(7) (2013) pp. 221-227.
9. P. V. Dhanaraj, G. Bhagavannarayana and N. P. Rajesh, *Mater. Chem. Phys.*, **112**(2) (2008) pp. 490-495.
10. M. Meena and C. K. Mahadevan, *Cryst. Res. Tech.*, **43**(2) (2006) pp. 166-172.
11. K. D. Parikh, D. J. Dave, B. B. Parekh and M. J. Joshi, *Cryst. Res. Tech.*, **45**(6) (2010) pp. 603-610.
12. P. M. Ushasree, R. Jayaval, P. Ramasamy, *Mater. Chem. Phys.*, **61**(3) (1999) pp. 270-274.
13. J. Thomas Joseph Prakash, M. Lawrence, *Int. Jr. Comp. Appl.*, **8**(3) (2010) pp. 0975-8887.
14. N. R Dhumane, S. S. Hussaini, K. Dutta, P. Ghosh, and M. D. Shirsat, *Recent research in Science and technology*, **2**(10) (2010) pp. 30-34.
15. K. Senthil Kannan, S. Gunasekaran and Seethalakshmi, *Int. Jr. Sci. & Engg. Res.*, **4**(2) (2013) pp. 1-5.
16. K. Kanagasabapathy, R. Rajasekaran, *Optoelectronics and Adv. Mater. - rapid Commu.*, **6**(1-2) (2012) pp. 218-224.
17. N. R. Dhumane, S. S. Hussaini, V. G. Dongre, M. D. Shirsat, *Opt. Mater.*, **31**(2) (2008) pp. 328–332.
18. P. M. Ushasree, R. Jayaval, P. Ramasamy, *Mater. Sci. Eng. B.*, **65**(3) (1999) pp. 153-158.
19. S. Aruna, G. Bhagavannarayana, M. Palanisamy, P. C. Thomas, B. Varghese and P. Sagayaraj, *J. Cryst. Growth*, **300**(2) (2007) pp. 403-408.
20. S. Boomadevi, H. P. Mittal and R. Dhansekaran, *J. Cryst. Growth*, **26**(1) (2004) pp. 55-62.
21. S. Suresh, A. Ramanand, D. Jayaraman and P. Mani, *Optoelectronics and Advanced Materials*, **4**(11) (2010) pp. 1763-1765.
22. C. Balarew and R. Duhlew, *J. Solid State Chem.*, **55**(1) (1984) pp. 1-6.

23. K. Funke, *Prog. Solid State Chem.*, **22**(2) (1993) pp. 111-195.

24. A. K. Jonscher, *Nature*, **267** (1977) pp. 673-679.

25. D. P. Almond and C. R. Bowen, *Phys. Rev. Lett.,* **92**(15) (2004) pp. 157601(1-4).

26. Z. Imran, M. A. Rafiq, M. Ahmad, K. Rasool, S. S. Batool, M. M. Hasan, *AIP Adv.*, **3** (2013) pp. 032146.

27. M. A. Afifi, A. E. Berkheet, E. Elwahabb, H. E. Atvia, *Vacuum*, **61**(1) (2001) pp. 9-17.

28. Chen Chuang-tian, Liu Guang-Zhao, *Ann. Rev. Mater. Sci.*, **16** (1986) pp. 203-243.

29. Lin Zheshuai, Wang Zhizhong, Chen Chungtian, Lee Ming-Hsien. *J. Chem. Phys.*, **118**(5) (2003) pp. 2349-2356.

R. A. Ganeev, I. A. Kulagin, A. I. Ryasnyansky, R. I. Tugushev, T. Usmanov, *Opt. Commun.*, **229** (2004) pp. 403-412.